BNL-225574-2024-JAAM

Understanding improved cycling and thermal stability of compositionally graded Ni-rich layered LiNi0.6Mn0.2Co0.2O2 cathode materials

S. Bak, J. T. Sadowski

To be published in "Nano Energy"

April 2024

Center for Functional Nanomaterials

Brookhaven National Laboratory

U.S. Department of Energy

USDOE Office of Science (SC), Basic Energy Sciences (BES). Scientific User Facilities (SUF)

DISCLAIMER

Understanding improved cycling and thermal stability of compositionally graded Ni-rich layered $LiNi_{0.6}Mn_{0.2}Co_{0.2}O_2$ cathode materials

Seong-Min Bak[a,*], Myeongjun Song[a], Zulipiya Shadike[b], Adrian Hunt[c], Iradwikanari Waluyo[c], Jerzy T. Sadowski[d], Hanfei Yan[c], Yong S. Chu[c], Xiao-Qing Yang[e], Xiaojing Huang[c,*], and Youngho Shin[f,*]

[a] Department of Materials Science and Engineering, Yonsei University, Seoul 03722, Republic of Korea
[b] Institute of Fuel Cells, School of Mechanical Engineering, Shanghai Jia Tong University, Shanghai 200240, P. R. China
[c] National Synchrotron Light Source II, Brookhaven National Laboratory, Upton, New York 11973, United States
[d] Center for Functional Nanomaterials, Brookhaven National Laboratory, Upton, New York 11973, United States
[e] Chemistry Division, Brookhaven National Laboratory, Upton, New York 11973, United States
[f] Materials Engineering Research Facility, Applied Materials Division, Argonne National Laboratory, Lemont, Illinois 60439, United States

*Corresponding authors
E-mail address: smbak@yonsei.ac.kr (S.-M. Bak), xhuang@bnl.gov (X. Huang), yshin@anl.gov (Y. Shin)

Abstract
The concentration gradient is a strategic design, adjusting the distribution of Ni, typically with a higher Ni content in the core and a higher Mn content toward the surface. This design leverages the pivotal role of the Ni/Mn ratio, seeking to optimize cathode performance by balancing Ni's high capacity with Mn's stabilizing effects, particularly at the surface where degradation commonly occurs during cycling. Our study delves into the intricate structural and chemical transformations within concentration gradient cathode materials during electrochemical cycling. Utilizing advanced synchrotron X-ray techniques, including hard and soft X-ray absorption spectroscopy (hXAS, sXAS), and nanoscale X-ray imaging, we investigate buried changes in concentration gradient $LiNi_{0.6}Mn_{0.2}Co_{0.2}O_2$ (CG NMC622). Contrary to conventional assumptions, our findings challenge the notion that cycling stability relies solely on Mn stability. Unraveling the roles of Ni and Mn, we uncover how their individual and collective contributions impact the cathode's overall performance. This investigation transcends established paradigms, shedding light on the crucial mechanisms governing the enhanced cycling stability of Ni-rich layered cathode materials.

Keywords: Ni-rich layered oxide, concentration gradient cathode, long cycling, thermal stability, synchrotron x-ray characterizations

1. Introduction

Pursuing cathode materials with improved energy density, cycling stability, and safety is pivotal for advancing lithium-ion battery (LIB) technology for electrical vehicle (EV) applications. Among the promising candidates, the nickel-rich layered oxides, exemplified by $LiNi_xMn_yCo_zO_2$ (NMC, x+y+z = 1, x >0.6), have emerged as leading contenders due to their high capacity. [1-3] However, challenges associated with capacity degradation over cycling and thermal instability worsen when Ni content increases, spurring innovative strategies to enhance their performance.

Previous studies of NMC materials reveal that the composition of Ni and Mn is a key parameter to control the capacity and safety of this materials system. It can be highlighted that Ni is more responsible for the specific capacity of NMC, while Mn plays a crucial role in enhancing thermal stability and improving the safety performance of the LIBs.[4-6] However, Mn's limited electrochemical redox activity during cycling creates a dilemma where increasing Mn for safety compromises the capacity of NMC. This trade-off necessitates carefully optimizing the Ni/Mn ratio in NMC materials. This establishes a fundamental guideline for the design of NMC systems, where the Ni/Mn ratio is controlled to obtain the required performance of NMC cathode material. [7, 8]

While the overall properties of NMC are governed mainly by the Ni/Mn ratio, the performance degradation of Ni-rich NMC is also affected by the surface/interfacial structural changes during the electrochemical cycling. It is known that the degradation of Ni-rich NMC occurs more severely at the surface of NMC particles and propagates into the bulk structure. [9-11] Furthermore, the chemo-mechanical degradation associated with creating the micro-cracks of the secondary particle of NMC is considered one of the most problematic degradation mechanisms. [12-14] Once micro-cracking happens at the NMC, it generates new exposing interfaces and induces more surface/interfacial reaction, resulting in capacity decay of the cathode over cycling. [13]

Therefore, for developing Ni-rich NMC cathode with high capacity and better safety, controlling the bulk composition (i.e., Ni/Mn ratio) and stabilizing the surface with stable oxide coating [15] or elemental doping[16-18] is commonly required for improving the overall performance of Ni-rich NMC cathode materials.

Among various approaches to NMC materials design, a notable approach involves the creation of compositional gradients within Ni-rich NMC cathode materials, where a tailored distribution of nickel is introduced across the particle, resulting in a manganese-rich surface and a nickel-rich core structure.[19, 20] This approach is considered one of the best strategies to gain high capacity with improved cycling stability and safety performance of Ni-rich NMC because the Ni content highly set in overall concentration can provide high capacity while the Mn-rich surface can enhance stability from the surface. [19] While previous studies have proposed the stabilizing role of the manganese-rich surface, attributing the overall stability to this configuration, the fundamental mechanism underlying this enhancement demands a more nuanced exploration.

In this study, we embark on a comprehensive investigation into the intricacies of the enhanced cycling stability observed in compositionally graded $LiNi_{0.6}Mn_{0.2}Co_{0.2}O_2$ (NMC622) layered cathodes. Our focus lies in elucidating the "buried" structure/chemical changes and understanding its fundamental mechanisms, particularly the contributions of the manganese-rich surface and the nickel-rich core to the overall performance of this class of materials.

Employing advanced synchrotron X-ray characterization techniques, including hard X-

ray absorption spectroscopy (hXAS), soft X-ray absorption spectroscopy (sXAS), and nanoscale X-ray imaging, we delve into the structural and chemical changes occurring within the Ni-rich NMC cathode materials during electrochemical cycling. This study aims to move beyond conventional wisdom and provide a deeper understanding of the stabilizing mechanisms of concentration gradient cathode, shedding light on Ni and Mn's individual and collective roles in imparting cycling stability.

2. Result and discussion

2.1. Compositional elemental analysis of CG NMC622 and electrochemical test

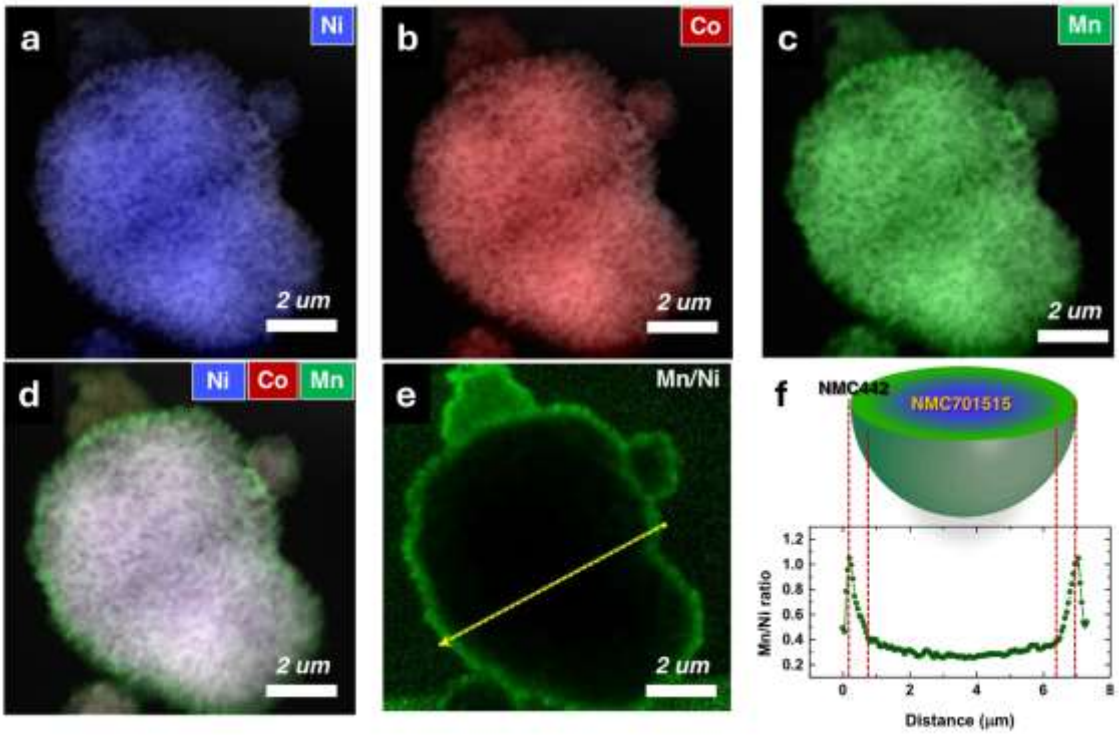

Fig.1. Nanoscale XRF imaging of randomly selected CG NMC622 particle. (a-c) Compositional elemental mapping of Ni, Co, and Mn, respectively. (d) overlayed image of Ni, Co, Mn, (e) calculated image that Mn divided by Ni composition, providing a sense of core-shell type structure with the Mn-rich surface, and (f) the Mn/Ni ratio profiles across the CG NMC622 particle along the yellow line presented in Fig.1e.

Figure 1 shows the nanoscale X-ray fluorescence (XRF) imaging result of the pristine concentration gradient NMC622 (CG NMC622) cathode material with a hard X-ray nanoprobe [21, 22], used in this study. The elemental-specific XRF images for Ni, Co, and Mn confirmed the core-shell type compositional heterogeneity with Mn-rich surface structure in the pristine CG NMC622 (Figure 1a-d). The image after processes by dividing Mn contents by Ni contents (Figure 1e) provides a clear core-shell structure of CG-NMC622 particle. With a line scan with an indication with a yellow arrow in Fig. 1e, we could evaluate the Mn/Ni ratio changes across the particle. Based on this measurement, the CG-NMC622 cathode materials used in this study have a concentration gradient structure composing an Mn-rich surface corresponding to $LiNi_{0.4}Mn_{0.4}Co_{0.2}O_2$ (NMC442) and Ni-rich core corresponding to $LiNi_{0.7}Mn_{0.15}Co_{0.15}O_2$ (NMC701515) composition

(Figure 1f). As indicated in the Mn/Ni ratio profile in Fig.1f, there is a compositional gradient region that appears as a gradual change of Mn/Ni ratio within 1um thickness in between the Mn-rich surface (NMC442) and Ni-rich core (NMC701515), that confirms concentration gradient of the pristine CG NMC622. The XRF imaging for multi-particles confirms that this CG NMC622 is representative. (Supplementary Figure 1s). It is worth noting that the nanoscale XRF imaging in Fig. 1 and 1s has advantages over electron microscopy, which usually applies to this class of materials in the literature. [23-25] The measurement especially does not involve any sample destructive processes such as cross-sectioning with ion milling. So, there is no concern about material deformation during the process; it provides more preserved information from the samples. Moreover, it also provides a more accurate quantitative analysis of the elemental composition of particles from single particle to multiple particle level. Since the CG NMC materials have a compositional heterogeneity in the nanometer scale, nanoscale XRF imaging in this study is compelling to study this class of materials.

To study the stabilizing mechanisms of CG-NMC622 cathode materials, we compared the conventional NMC622 without concentration gradient, as a counterpart of CG-NMC622. As shown in Figure 2, the galvanostatic charge/discharge profiles of conventional NMC622 (Fig.2a) and CG-NMC622 (Fig. 2b) over 100 cycles demonstrate the improved cycling stability of CG-NMC622 compared to normal NMC622. In the dQ/dV analysis (supplementary information Figure S2), we could see the clear difference in oxidation peak change during the cycling between conventional and CG-NMC622. Over 60th cycles, the oxidation peak appears at around 3.8V, is shifted to the higher voltage region, and the peak vanishes drastically in conventional NMC622. However, the CG-NMC622 shows less change in the oxidation peak regarding voltage and intensity, indicating better cycling stability.

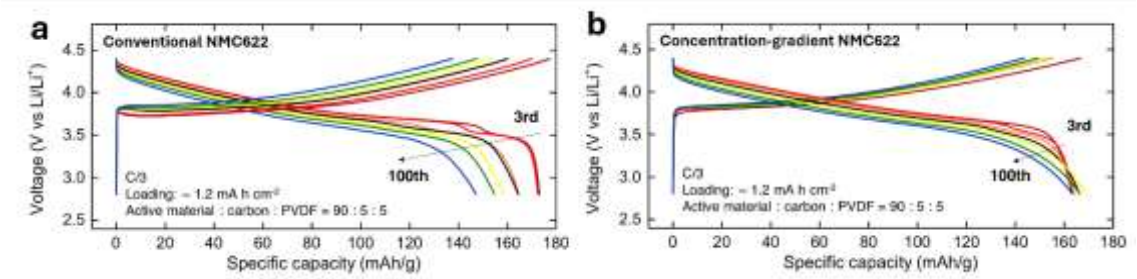

Fig. 2. Galvanostatic charge/discharge curves of (a) conventional NMC622 and (b) concentration-gradient NMC622 cathode cycled at C/3 rate in the voltage range of 2.7-4.4 V (vs. Li/Li$^+$).

2.2. Oxidation state changes of Ni and Mn in the bulk structure upon cycling

The decrease in capacity usually appears as the reduction in Ni-redox during the charge/discharge cycling since Ni is the main contributor to the capacity in the Ni-rich NMC system. [11] The degraded reversible capacity implies that Ni-redox contribution to the overall electrochemical charge storage is decreased. [26, 27]

Therefore, we first conducted hard X-ray absorption spectroscopy (hXAS) on the Ni K-edge to investigate changes in the Ni oxidation state after cycling. We primarily focus on the Ni K-edge X-ray absorption near edge structure (XANES), which provides the

oxidation state changes of Ni after 100 cycles, as shown in Figure 3a. All measurements were collected for the samples at the fully discharged state to consider whether the Ni oxidation state changed compared to the initial state of pristine NMC622.

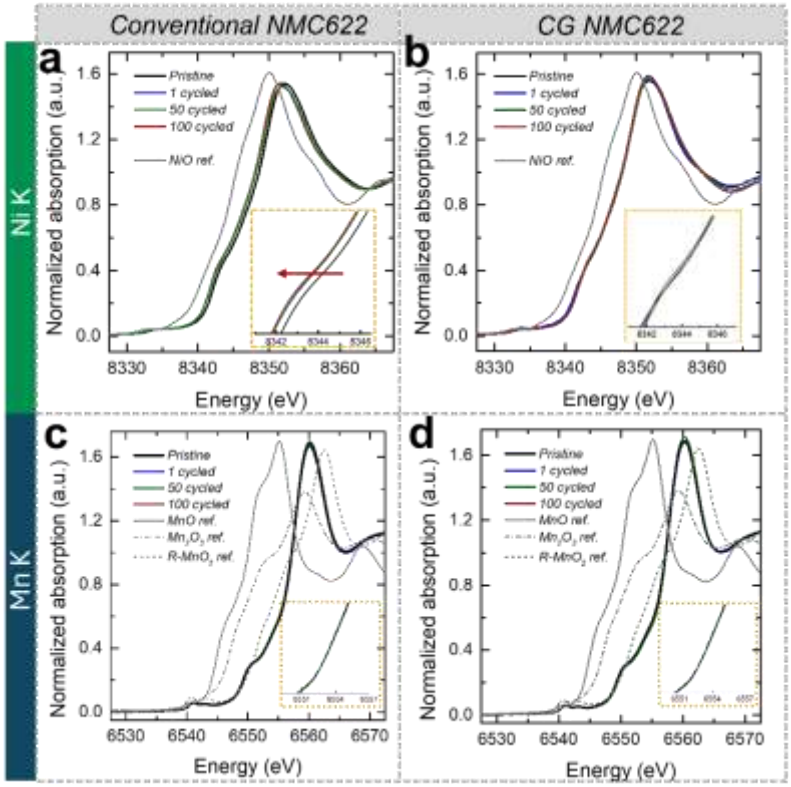

Fig. 3. Hard X-ray absorption spectroscopy (hXAS) of Ni and Mn K-edges for (a, c) conventional NMC622, and (b, d) CG-NMC622, respectively.

As a primary difference notably observed, the edge position of the Ni K-edge XANES spectra of normal NMC622 (Fig.3a) shifted after 100 cycles compared to the initial position for the pristine sample. The edge shift to lower energy here indicates a decrease in the Ni oxidation state. Since the average oxidation state of Ni in the NMC622 is about +2.67, this edge shift implies the increase of Ni^{2+}, resulting in the average oxidation state of Ni being below +2.67. As reported in the previous studies on the Ni-rich NMC cathode materials, the formation of Ni^{2+} is related to the irreversible phase transition, such as NiO rock-salt phases, resulting in the formation of an electrochemically inactive phase. [28-30] So, the formation of Ni^{2+} can be used as an indicator of an increase in irreversible Ni redox. [31, 32]

While normal NMC622 shows a reduction of Ni oxidation state, the CG NMC622 does not show notable changes in Ni K-edge XANES spectra (Fig. 3b). Because the main difference between normal and CG NMC622 is Ni and Mn composition, we also conducted Mn K-edge XANES, as shown in Figures 3c and d. All the Mn K-edge spectra were not changed over 100 cycles and were almost identical to the pristine states, agreeing with the previous knowledge about the stability of Mn in the NMC cathode.[31]

2.3. Surface oxidation state changes of Ni and Mn during the cycling

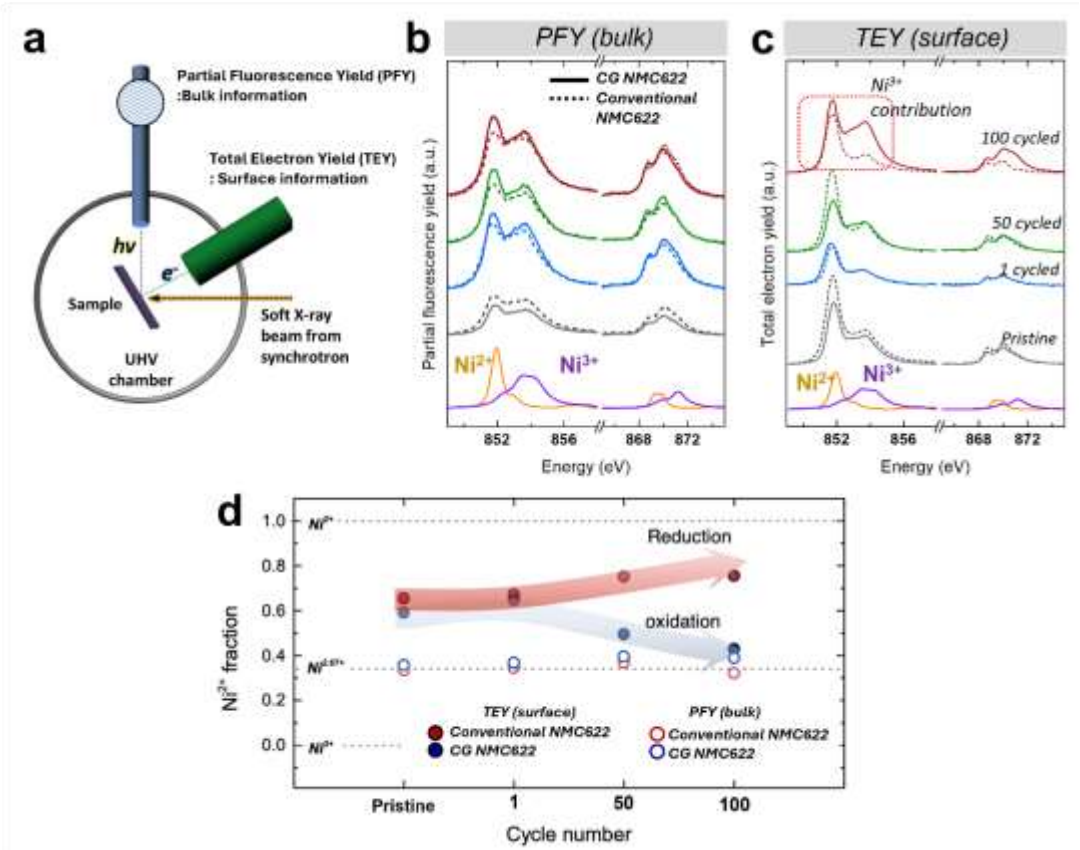

Fig.4. (a) The scheme of the sXAS setup illustrates that it provides simultaneous measurement of the partial fluorescence yield (PFY) and total electron yield (TEY), (b) PFY spectra, (c) TEY spectra for the conventional NMC622 and CG NMC622 for the pristine, 1, 50, 100 cycled electrodes. (d) Ni^{2+} fraction versus cycle numbers in the conventional NMC622 and CG NMC622 cathode display different valence state changes of Ni cation at the surface.

However, we should note that the hXAS provides averaged information on the bulk structure, which means that this characterization technique cannot provide distinguishable information on surface and bulk from the heterogeneous samples, such as concentration gradient cathode materials. Since the CG NMC622 has different Ni/Mn compositions and the electrochemical degradation of NMC622 is known to have happened differently at the surface and bulk, we conducted Ni $L_{2,3}$-edge soft X-ray absorption spectroscopy (sXAS), which can provide different Ni oxidation state information from the surface and bulk through different types of probing method with total electron yield (TEY) and partial fluorescence yield (PFY) modes, respectively. (Figure 4a). Figure 4b shows Ni $L_{2,3}$-edge sXAS results for the normal NMC622 (dashed line) and CG-NMC622 (solid line) collected in PFY mode, which is considered bulk information. The sXAS spectra for Ni^{2+} and Ni^{3+} from the standard sample (i.e., NiO and $LiNiO_2$, respectively) are also displayed for comparison. The spectral shape of the PFY sXAS from both samples can be considered a mixed state of Ni^{2+} and Ni^{3+} in a certain ratio, as it is supposed to have an average oxidation state of about +2.67. It does not show notable differences between normal and CG samples over 100 cycles, which means the

Ni oxidation state does not obviously change in the bulk structure. This is not coincident with the Ni K-edge XANES result in Fig 3a for the normal NMC622 case, which shows the noticeable Ni reduction. We will discuss the reason for this in the following session. Interestingly, there is a significant difference between conventional NMC622 and CG NMC622 samples after 100 cycles in the TEY spectra (Figure 4c). The greater Ni^{3+} contribution for the CG NMC622 electrode is clearly seen in Fig. 4c. The Co $L_{2,3}$-edge sXAS in both TEY and PFY were also measured, and the result shows that a bit of Co^{2+} formed at the surface, whereas the bulk structure remains as Co^{3+} in both conventional and concentration gradient NMC622.

A linear combination fitting (LCF) analysis was conducted for Ni L_3-edge sXAS spectra to provide a more precise view of the Ni oxidation state (the fitting results are provided in the supplementary Figure S3). Figure 4d illustrates the Ni^{2+} fraction in each sXAS spectrum for both conventional NMC622 and CG NMC622, determined through LCF analysis. When we compare the TEY and PFY, we can see that the TEY result shows a slightly higher Ni^{2+} content. The reason for this result is not apparent, but it might be associated with a low Ni valence structure formation at the surface region introduced during the lithiation process. [33] In the case of normal NMC622, a noticeable rise in Ni^{2+} contribution was observed during cycling, consistent with the Ni K-edge XANES results depicted in Fig. 3a. It is noteworthy that the formation of Ni^{2+} (indicative of the creation of NiO-type rock-salt phase) predominantly occurs at the surface. Interestingly, an unexpected trend in Ni oxidation state change was observed from the CG-NMC622 cathode. In the case of CG NMC622, the oxidation state of Ni is even slightly increased (i.e., the Ni^{2+} contribution decreased). This trend in Ni oxidation state change at the surface of CG-NMC622 is repeated in the X-ray photon emission electron microscopy (XPEEM), a surface-sensitive spectromicroscopy technique, as shown in Figure S4.

The mitigation of electrochemically inactive Ni^{2+} formation on the surface of CG-NMC622 suggests the preservation of active Ni-redox species, potentially enhancing cycling performance. However, the reason behind the increased Ni oxidation state on the CG-NMC622 cathode surface remains unclear. To explore this, we conducted Mn L-edge sXAS to investigate any changes in the Mn oxidation states, as illustrated in Figure 5. Reference spectra collected from standard oxides for Mn^{2+}, Mn^{3+}, and Mn^{4+} (i.e., MnO, Mn_2O_3, and MnO_2, respectively) are also included for comparison. Given the stability of Mn observed in the hXAS result (Fig. 3c-d), significant alterations in Mn oxidation states were not anticipated. As shown in Fig. 5a, the PFY spectra of Mn $L_{2,3}$-edge sXAS for both normal and CG NMC622 cathode do not change for cycled samples and stay as Mn^{4+}, which coincident with the hXAS result in Fig 3c-d. Surprisingly, however, the Mn spectra collected in TEY mode (Figure 5b) show a significant spectral change as the cycling numbers increase for both cathodes. The Mn^{2+} contribution is significantly increased for the 100 cycled samples in both conventional NMC622 and CG NMC622 cathode, implying a reduction of the Mn valence state at the surface during the electrochemical cycling.

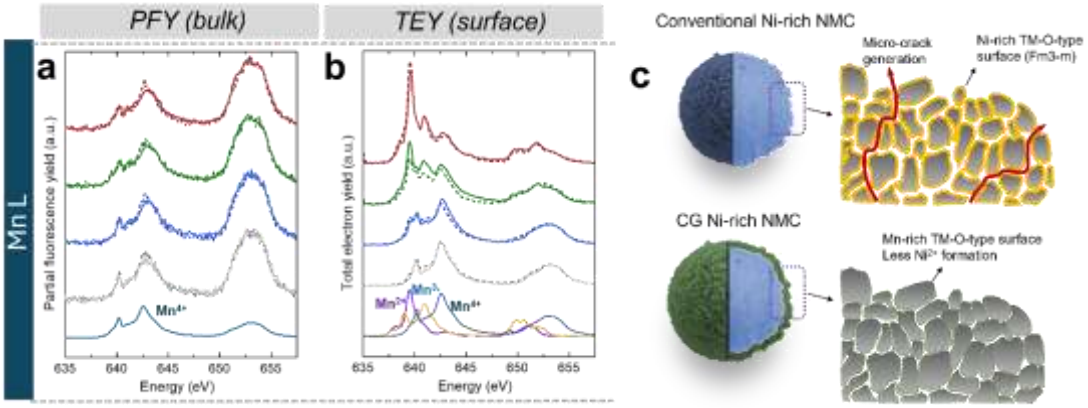

Fig. 5. Mn $L_{2,3}$-edge sXAS spectra of (a) PFY and (b) TEY measurement for conventional NMC622 (dashed line) and CG NMC622 (solid line). (c) schematic illustration demonstrates a difference in structural degradation mechanism between conventional NMC622 and CG NMC622.

2.3. Discussion on the mechanism of improved cycling stability of CG NMC622

The reduction process from Mn^{4+} to Mn^{2+} involves a gain of two electrons for the system, while Ni^{2+} formation involves a process of losing one electron. The Mn content at the surface of conventional NMC622 and CG NMC622 is 0.2 and 0.4, respectively, whereas the Ni content is 0.6 and 0.4, respectively. We can make a simple approximation to balance the charge of Ni and Mn to maintain the charge neutrality of the entire system, as outlined below:

1) For the conventional NMC622
   - The electron gained from Mn^{4+} to Mn^{2+} process: $0.2 \times 2 = 0.4$
   - The electron lost from Ni^{3+} to Ni^{2+} process: $0.6 \times 1 = 0.6$

2) For the CG NMC622
   - The electron gained from the Mn^{4+} to Mn^{2+} process: $0.4 \times 2 = 0.8$
   - The electron lost from Ni^{3+} to Ni^{2+} process: $0.4 \times 1 = 0.4$

Based on the above consideration, for the conventional NMC622, the Ni oxidation state needs to be decreased to make charge neutrality, while the Ni oxidation state needs to be increased for the CG NMC622. Because a larger amount of Mn is involved in the surface of CG NMC622, and the amount of charge change is more significant than that for the conventional NMC622, the system prefers to increase the Ni valence state to maintain charge neutrality. This might help the CG NMC622 keep electroactive phases compared to conventional NMC622 samples.

Hence, the enhanced cycling stability of CG NMC622 is linked to the Ni/Mn ratio. However, the underlying mechanism challenges the conventional belief derived from previous studies, which assumed that the improved cycling stability is solely dependent on the stability of Mn. More precisely, the Mn-rich surface helps maintain the Ni redox active phases at the surface, although it is also formed into reduced phases the same way Ni gets reduced into Ni^{2+} at the Ni-rich surface. This might be associated with a surface reconstruction process to form a cubic phase at the surface of the NMC particle.

[10] The formation of surface stable structures is not evitable during the cycling, but less irreversible Ni^{2+} formation of CG NMC622 has a significant advantage for stabilizing the structure of NMC secondary particle since the lattice expansion/contraction, which induces a chemo-mechanical degradation in secondary particle level is much affected by Ni oxidation state changes during the cycling. [11, 12] Once the surface is stabilized with an Mn-O type structure, irreversible Ni^{2+} formation is prevented, and the irreversible phase formation, which results in irreversible capacity loss, is also mitigated. Mn-rich composition at the surface seemed to induce different surface reconstruction pathways and maintained Ni redox activity at the surface/sub-surface. This stabilizes the secondary particle structure and suppresses the formation of structure degradation initiators such as nanopores and micro/nanocracks. (Fig.5c)

To probe whether the concentration gradient is still retained after charge/discharge cycles, we performed nanoscale XRF imaging for multiple particles after 100 cycles with a regular cut-off voltage of 4.4V and a high cut-off voltage of 4.8V (Supplementary Figure S5). In both cases, the Mn-rich surface structure is preserved. This result indicates that the interdiffusion mixing of Ni/Mn does not occur while their valence state changes at the surface. In this study, it is difficult to fully understand the surface/or sub-surface structure differences between conventional NMC622 and CG NMC622, and it remained a future work to be studied with atomic scale structure investigation with high-resolution transmission electron microscope coupled with chemical analysis such as electron energy loss spectroscopy (EELS), phase/strain analysis with X-ray coherent diffraction imaging (CDI), and nanoscale XANES imaging. [34]

2.4. Thermal stability study on CG NMC622

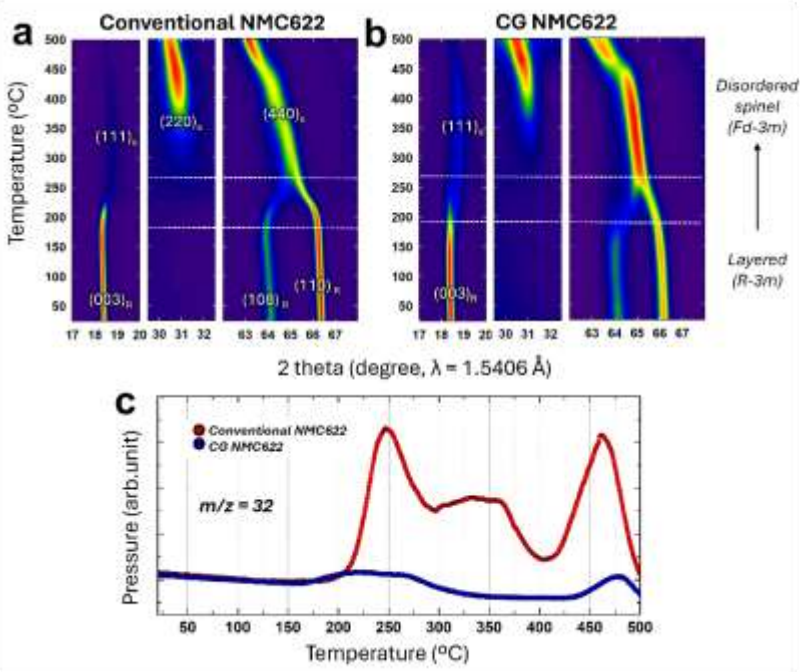

Fig. 6. Contour plot of the time-resolved X-ray diffraction (TR-XRD) patterns at the selected 2θ range of the (a) charged conventional NMC622 and (b) charged CG NMC622 cathode materials during in situ heating to 500 ºC. (c) O_2 (m/z=32) released from conventional NMC622 and CG NMC622 during in situ heating to 500 ºC.

The thermal stability of cathode materials is crucial for the safety characteristics of lithium-ion batteries (LIBs), particularly in electric vehicle (EV) applications. To investigate the thermal stability of CG NMC622, in situ time-resolved X-ray diffraction coupled with mass spectroscopy (TR-XRD/MS) studies during heating were conducted. It is noteworthy that the structure degradation observed during heating mirrors the phase transition observed during prolonged electrochemical cycling. The degradation of the structure can be accelerated during heating, making the information on structural changes obtained through thermal decomposition studies a valuable reference that simulates the conditions of extensive electrochemical cycling in a short time.[33] This aspect is particularly useful when conducting in situ studies with limited synchrotron beam time.

For comparison, both conventional NMC622 and CG NMC622 materials were studied. They were cycled in 2032 coin cells between 2.7 and 4.4V for 99 cycles and then charged to 4.4V at the 50th cycle. Galvanostatic at C/10 rate for the first three cycles and C/3 for the following 97 cycles were applied to the coin cells. Contour plot of the TR-XRD patterns at the selected 2θ ranges for the conventional NMC622 and CG NMC622 during heating to 500 ºC are shown in Fig. 6a and b, respectively (at a heating rate of ~4 ºC/min). Both samples showed that at a charged state (4.4V) after 100 cycles, the crystal structure was retained in the layered structure of rhombohedral ($R\bar{3}m$). During the heating, both cathode materials showed a phase transition from layered structure to disordered spinel ($Fd\bar{3}m$) as a result of thermal decomposition, as reported in previous studies. [5, 35] The appearance of $(220)_S$ peak and disappearance of $(003)_R$ peak with the merging of $(108)_R/(110)_R$ peak indicate the occurrence of phase transition from a layered structure to a disordered spinel structure, which accompanying with oxygen (O_2) release (Fig. 6c) during the heating. [5, 33, 35] As is shown in Fig. 6a, b, the temperature of first thermal decomposition and phase transformation from the layered to disordered spinel phase are similar. This might be because the thermal decomposition behavior of Ni-rich layered oxide is governed by bulk structure property. Thus, the conventional NMC622 and CG NMC622 show similar thermal stability due to the overall concentration of Ni being the same level.

However, very interestingly, the O_2 release behavior is observed in a large contrast, as shown in Fig. 6c. For the charged conventional NMC622 cathode, a sharp O_2 release begins when the phase transition from the layered to the disordered spinel phase occurs at around 190 ºC. The peak-shaped O_2 release behavior is often observed from the Ni-rich cathode (e.g., $LiNi_{0.8}Co_{0.15}Al_{0.05}O_2$ (NCA), NMC811, NMC 622) at a highly charged state (e.g., overcharged). The sharp O_2 release at low temperatures would definitely cause serious safety problems. In LIBs at a practical level, where a large amount of highly reductive electrolyte is available, the pulse of highly reactive oxygen species released from the cathode can quickly react with the flammable electrolyte and accelerate the thermal runaway. The previous studies on NCA and NMC materials by Bak et al. suggest that suppressing the oxygen release, pushing its starting point to higher temperatures, and spreading its reaction to a wider temperature range are critical to improving the safety characteristic of LIBs.[5, 35] Interestingly, charged CG NMC622 does not show such a peak-shaped O_2 release behavior and spreads through a wider temperature range. This might help to mitigate the acceleration of the thermal runaway. This result implies that the Mn-rich and surface structure formed with reduced Mn cation and electroactive Ni-

redox phase suppresses the O_2 release and effectively stabilizes the structure.

3. Conclusion

Our comprehensive investigation, employing synchrotron nanoscale X-ray imaging, and hard and soft X-ray absorption spectroscopy techniques, has unraveled the intricate mechanisms contributing to the improved cycling stability of concentration-gradient NMC622 cathode materials. The observed enhanced cycling stability of CG NMC622, in comparison to conventional NMC622, is a result of nuanced interactions at multiple scales. In Ni-rich cathodes, the formation of inactive Ni^{2+} during cycling, particularly at the surface, is a common challenge. Our analysis, integrating Ni and Mn L-edge sXAS, indicates that the Mn-rich surface of CG NMC622 plays a pivotal role in maintaining Ni redox active phases, despite Mn^{4+} reduction to Mn^{2+} and the formation of Ni^{2+} in the Ni-rich surface. This underscores the significance of the Ni/Mn ratio, but our findings go beyond the conventional assumption that cycling stability is not solely contingent on manganese stability. The stabilized Mn-O-rich structure on the surface of CG NMC622 proves instrumental in mitigating irreversible Ni^{2+} formation, as confirmed by TR-XRD/MS analysis. Notably, this enhanced stability also translates into improved thermal performance, with CG NMC622 exhibiting a gentler oxygen release compared to the conventional counterpart. This revelation hints at broader possibilities, suggesting that other high-valence state elements with facile oxide formation might offer avenues to stabilize the surface of Ni-rich layered cathodes without incurring the issue of inactive Ni^{2+} formation. In essence, our study provides not only a deeper understanding of the intricacies governing the cycling stability of concentration-gradient NMC622 cathode materials but also opens new avenues for the design of high-performance cathodes crucial for advancing lithium-ion battery technology.

4. Experimental Section

Materials synthesis. Normal NMC622 (Targray) was used as the manufacturer provided it. Concentration gradient structured hydroxide precursor with an average composition of $[Ni_{0.6}Mn_{0.2}Co_{0.2}](OH)_2$ were synthesized via the co-precipitation method using a 20L batch reactor. $NiSO_4 \cdot 6H_2O$, $CoSO_4 \cdot 7H_2O$, $MnSO_4 \cdot 5H_2O$, NaOH, and NH_4OH were used as starting materials. The prepared $[Ni_{0.6}Mn_{0.2}Co_{0.2}](OH)_2$ precursor was filtered, washed, and dried for 20 h at 100 ˚C. The dried precursor was mixed with $LiOH \cdot H_2O$, and portions of the mixture were calcined at 800 ˚C for 20 h under oxygen flow. Details of the synthesis method are described in the previous reports.[33, 36]

Electrochemical measurement. The electrode was prepared by a slurry coating of a mixture of active materials ($LiNi_{0.6}Co_{0.2}Mn_{0.2}O_2$): acetylene black: polyvinylidene fluoride binder in 90:5:5 weight ratio, onto Al foil. The electrode was dried at 80 ºC in a vacuum overnight before use. The loading amount of NMC622 electrode is controlled at about 6.5 mg/cm^2, and ca. 75 uL of electrolyte was used for the cell testing. The 2032-type coin cells were assembled in an argon-filled glove box with lithium metal as the anode and a celgard as the separator. The electrolyte was 1.0 M $LiPF_6$ dissolved in ethylene carbonate and dimethyl carbonate solvent (3:7 by volume) SP-300 potentiostat/galvanostat (Biologic SA, France) and MACCOR battery cycler (Maccor,

Inc., Tulsa) was used for electrochemical testing.

Hard X-ray Nanoprobe. The nanoscale XRF imaging was performed at the Hard X-ray Nanoprobe Beamline (HXN, 3-ID) of the National Synchrotron Light Source II (NSLS-II) at Brookhaven National Laboratory (BNL) [21, 22]. The incident X-ray energy was set to 9 keV. The microscope sits about 15 m downstream from the secondary source aperture (SSA), and a Fresnel zone plate (Applied Nanotools Inc.) with 30 nm outmost zone width was used to focus the beam to a nano spot. An energy-dispersive detector (Vortex, Hitach) was placed at 90º horizontally with respect to the sample to collect fluorescence signals. The XRF imaging data were processed using PyXRF.[37]

X-ray absorption spectroscopy. The hard XAS experiment was carried out at QAS (7-BM) beamline of the NSLS-II at BNL. All spectra were collected in transmission mode. The beam intensity was detuned to 35-40 % of its initial intensity to minimize the high-order harmonics. Reference spectra of metallic were collected simultaneously with all of the spectra for energy calibration. The energy calibration was carried out using the first inflection point of the K-edge spectrum of transition metal foil as a reference. The XANES and EXAFS data were analyzed using the ATHENA software package. [38]
The soft XAS measurement was collected by using both total electron yield (TEY) through drain current measurements and partial fluorescence yield (PFY) modes at the IOS (23-ID-2) beamline of NSLS-II at BNL. PFY spectra were collected using a Vortex silicon drift detector. All the soft XAS measurements were performed at room temperature in the ultrahigh-vacuum chamber (base pressure, ~ 10^{-9} torr). A more detailed description of the beamline and end station can be found elsewhere. [39]

X-ray photon emission electron microscopy. The XPEEM was carried out at the XPEEM endstation of the Electron Spectro-Microscopy (ESM) beamline (21-ID) of the NSLS-II at BNL. All the experiments were performed in an ultra-high vacuum (base pressure, ~ 3 x 10^{-10} torr) at room temperature. The absorption spectra are obtained by recording a sequence of XPEEM images as a function of photon energy linearly polarized light. All the spectra are normalized by the incoming flux measured from a gold mesh.

In situ time-resolved XRD and mass spectroscopy. In situ TR-XRD data were collected at beamline 17-BM-B (λ = 0.45220 Å) of the Advanced Photon Source (APS) at Argonne National Laboratory. The details of the sample preparation and experimental setup have been published previously.[35] TR-XRD patterns (~1 min for each XRD scan) and MS signal were simultaneously collected continuously as the sample was heated from room temperature to 500 °C for 2 h (i.e., at a heating rate of ~4 °C min^{-1}). For easy comparison with results in the literature, the 2θ angles have been converted to values corresponding to the Cu Kα radiation (λ = 1.5406 Å).

Declaration of Competing Interest
The authors declare that they have no known competing financial interests or personal relationships that could have appeared to influence the work reported in this paper.

Acknowledgments

The work was supported by the Assistant Secretary for Energy Efficiency and Renewable Energy, Vehicle Technology Office of the U.S. Department of Energy through the Advanced Battery Materials Research (BMR) Program, including Battery500 Consortium under Contract DE-SC0012704. Y. Shin was supported by the Office of Vehicle Technologies of the U. S. Department of Energy under contract number DE-AC02-06CH11357. S.-M. Bak acknowledges the Yonsei University Research Fund of 2023-22-0158. This research used resources 3-ID, 7-BM, 21-ID, and 23-ID-2 of the National Synchrotron Light Source II, a U.S. Department of Energy (DOE) Office of Science User Facility operated for the DOE Office of Science by Brookhaven National Laboratory under Contract No. DE-SC0012704. This research used resources of the Center for Functional Nanomaterials, which is a U.S. DOE Office of Science Facility, and the Scientific Data and Computing Center, a component of the Computational Science Initiative, at Brookhaven National Laboratory under Contract No. DE-SC0012704. The TR-XRD/MS experiments were carried out at Beamline 17-BM-B of the Advanced Photon Source (APS) which is supported by the U.S. Department of Energy, Office of Science, and Office of Basic Energy Science, under Contract No. DE-AC02-06CH11357.

References

[1] S.-T. Myung, F. Maglia, K.-J. Park, C.S. Yoon, P. Lamp, S.-J. Kim, Y.-K. Sun, Nickel-Rich Layered Cathode Materials for Automotive Lithium-Ion Batteries: Achievements and Perspectives, ACS Energy Letters 2(1) (2017) 196-223.

[2] R. Jung, F. Linsenmann, R. Thomas, J. Wandt, S. Solchenbach, F. Maglia, C. Stinner, M. Tromp, H.A. Gasteiger, Nickel, Manganese, and Cobalt Dissolution from Ni-Rich NMC and Their Effects on NMC622-Graphite Cells, Journal of The Electrochemical Society 166(2) (2019) A378.

[3] A. Manthiram, A reflection on lithium-ion battery cathode chemistry, Nature Communications 11(1) (2020) 1550.

[4] H.J. Noh, S. Youn, C.S. Yoon, Y.K. Sun, Comparison of the structural and electrochemical properties of layered $Li[Ni_xCo_yMn_z]O_2$(x=1/3, 0.5, 0.6, 0.7, 0.8 and 0.85) cathode material for lithium-ion batteries, J Power Sources 233 (2013) 121-130.

[5] S.-M. Bak, E. Hu, Y. Zhou, X. Yu, S.D. Senanayake, S.-J. Cho, K.-B. Kim, K.Y. Chung, X.-Q. Yang, K.-W. Nam, Structural changes and thermal stability of charged $LiNi_xMn_yCo_zO_2$ cathode materials studied by combined in situ time-resolved XRD and mass spectroscopy, ACS applied materials & interfaces 6(24) (2014) 22594-22601.

[6] J. Choi, A. Manthiram, Role of Chemical and Structural Stabilities on the Electrochemical Properties of Layered $LiNi_{1/3}Mn_{1/3}Co_{1/3}O_2$ Cathodes, Journal of The Electrochemical Society 152(9) (2005) A1714.

[7] N. Kosova, E. Devyatkina, V. Kaichev, Optimization of Ni^{2+}/Ni^{3+} ratio in layered Li (Ni, Mn, Co) O_2 cathodes for better electrochemistry, J Power Sources 174(2) (2007) 965-969.

[8] K.A. Jarvis, C.-C. Wang, A. Manthiram, P.J. Ferreira, The role of composition in the atomic structure, oxygen loss, and capacity of layered Li–Mn–Ni oxide cathodes, Journal of Materials Chemistry A 2(5) (2014) 1353-1362.

[9] K.W. Nam, S.M. Bak, E. Hu, X. Yu, Y. Zhou, X. Wang, L. Wu, Y. Zhu, K.Y. Chung, X.Q. Yang, Combining in situ synchrotron X-ray diffraction and absorption techniques

with transmission electron microscopy to study the origin of thermal instability in overcharged cathode materials for lithium-ion batteries, Advanced Functional Materials 23(8) (2013) 1047-1063.
[10] F. Lin, I.M. Markus, D. Nordlund, T.-C. Weng, M.D. Asta, H.L. Xin, M.M. Doeff, Surface reconstruction and chemical evolution of stoichiometric layered cathode materials for lithium-ion batteries, Nature Communications 5(1) (2014) 3529.
[11] H.-H. Ryu, K.-J. Park, C.S. Yoon, Y.-K. Sun, Capacity Fading of Ni-Rich $Li[Ni_xCo_yMn_{1-x-y}]O_2$ ($0.6 \leq x \leq 0.95$) Cathodes for High-Energy-Density Lithium-Ion Batteries: Bulk or Surface Degradation?, Chemistry of Materials 30(3) (2018) 1155-1163.
[12] S. Xia, L. Mu, Z. Xu, J. Wang, C. Wei, L. Liu, P. Pianetta, K. Zhao, X. Yu, F. Lin, Y. Liu, Chemomechanical interplay of layered cathode materials undergoing fast charging in lithium batteries, Nano Energy 53 (2018) 753-762.
[13] Y. Yang, R. Xu, K. Zhang, S.-J. Lee, L. Mu, P. Liu, C.K. Waters, S. Spence, Z. Xu, C. Wei, D.J. Kautz, Q. Yuan, Y. Dong, Y.-S. Yu, X. Xiao, H.-K. Lee, P. Pianetta, P. Cloetens, J.-S. Lee, K. Zhao, F. Lin, Y. Liu, Quantification of Heterogeneous Degradation in Li-Ion Batteries, Advanced Energy Materials 9(25) (2019) 1900674.
[14] P. Yan, J. Zheng, M. Gu, J. Xiao, J.-G. Zhang, C.-M. Wang, Intragranular cracking as a critical barrier for high-voltage usage of layer-structured cathode for lithium-ion batteries, Nature Communications 8(1) (2017) 14101.
[15] G. Kaur, B.D. Gates, Review—Surface Coatings for Cathodes in Lithium Ion Batteries: From Crystal Structures to Electrochemical Performance, Journal of The Electrochemical Society 169(4) (2022) 043504.
[16] S. Liu, Z. Dang, D. Liu, C. Zhang, T. Huang, A. Yu, Comparative studies of zirconium doping and coating on $LiNi_{0.6}Co_{0.2}Mn_{0.2}O_2$ cathode material at elevated temperatures, J Power Sources 396 (2018) 288-296.
[17] K.-J. Park, H.-G. Jung, L.-Y. Kuo, P. Kaghazchi, C.S. Yoon, Y.-K. Sun, Improved Cycling Stability of $Li[Ni_{0.90}Co_{0.05}Mn_{0.05}]O_2$ Through Microstructure Modification by Boron Doping for Li-Ion Batteries, Advanced Energy Materials 8(25) (2018) 1801202.
[18] F.A. Susai, A. Bano, S. Maiti, J. Grinblat, A. Chakraborty, H. Sclar, T. Kravchuk, A. Kondrakov, M. Tkachev, M. Talianker, D.T. Major, B. Markovsky, D. Aurbach, Stabilizing Ni-rich high energy cathodes for advanced lithium-ion batteries: the case of $LiNi_{0.9}Co_{0.1}O_2$, Journal of Materials Chemistry A 11(24) (2023) 12958-12972.
[19] Y.-K. Sun, S.-T. Myung, B.-C. Park, J. Prakash, I. Belharouak, K. Amine, High-energy cathode material for long-life and safe lithium batteries, Nature Materials 8(4) (2009) 320-324.
[20] Y.-K. Sun, S.-T. Myung, M.-H. Kim, J. Prakash, K. Amine, Synthesis and Characterization of $Li[(Ni_{0.8}Co_{0.1}Mn_{0.1})0.8(Ni_{0.5}Mn_{0.5})_{0.2}]O_2$ with the Microscale Core−Shell Structure as the Positive Electrode Material for Lithium Batteries, Journal of the American Chemical Society 127(38) (2005) 13411-13418.
[21] H.F. Yan, N. Bouet, J. Zhou, X.J. Huang, E. Nazaretski, W.H. Xu, A.P. Cocco, W.K.S. Chiu, K.S. Brinkman, Y.S. Chu, Multimodal hard x-ray imaging with resolution approaching 10 nm for studies in material science, Nano Futures 2(1) (2018).
[22] E. Nazaretski, H. Yan, K. Lauer, N. Bouet, X. Huang, W. Xu, J. Zhou, D. Shu, Y. Hwu, Y.S. Chu, Design and performance of an X-ray scanning microscope at the Hard X-ray Nanoprobe beamline of NSLS-II, J Synchrotron Radiat 24 (2017) 1113-1119.
[23] U.-H. Kim, J.-H. Kim, J.-Y. Hwang, H.-H. Ryu, C.S. Yoon, Y.-K. Sun, Compositionally and structurally redesigned high-energy Ni-rich layered cathode for

next-generation lithium batteries, Materials Today 23 (2019) 26-36.
[24] H.-H. Ryu, H.-W. Lim, G.-C. Kang, N.-Y. Park, Y.-K. Sun, Long-Lasting Ni-Rich NCMA Cathodes via Simultaneous Microstructural Refinement and Surface Modification, ACS Energy Letters 8(3) (2023) 1354-1361.
[25] Y. Mu, X. Chen, H. Ming, S. Zhang, X. Zhu, J. Qiu, Oriented Gradient Doping of Zirconium in Ni-Rich Cathode to Achieve Ultrahigh Stability and Rate Capability, ACS Applied Materials & Interfaces 15(42) (2023) 49289-49298.
[26] M. Jiang, D.L. Danilov, R.-A. Eichel, P.H.L. Notten, A Review of Degradation Mechanisms and Recent Achievements for Ni-Rich Cathode-Based Li-Ion Batteries, Advanced Energy Materials 11(48) (2021) 2103005.
[27] R. Jung, M. Metzger, F. Maglia, C. Stinner, H.A. Gasteiger, Oxygen Release and Its Effect on the Cycling Stability of $LiNi_xMn_yCo_zO_2$ (NMC) Cathode Materials for Li-Ion Batteries, Journal of The Electrochemical Society 164(7) (2017) A1361.
[28] H. Zhang, H. Liu, L.F.J. Piper, M.S. Whittingham, G. Zhou, Oxygen Loss in Layered Oxide Cathodes for Li-Ion Batteries: Mechanisms, Effects, and Mitigation, Chemical Reviews 122(6) (2022) 5641-5681.
[29] C. Xu, K. Märker, J. Lee, A. Mahadevegowda, P.J. Reeves, S.J. Day, M.F. Groh, S.P. Emge, C. Ducati, B. Layla Mehdi, C.C. Tang, C.P. Grey, Bulk fatigue induced by surface reconstruction in layered Ni-rich cathodes for Li-ion batteries, Nature Materials 20(1) (2021) 84-92.
[30] Z. Wang, Z. Wang, D. Xue, J. Zhao, X. Zhang, L. Geng, Y. Li, C. Du, J. Yao, X. Liu, Z. Rong, B. Guo, R. Fang, Y. Su, C. Delmas, S.J. Harris, M. Wagemaker, L. Zhang, Y. Tang, S. Zhang, L. Zhu, J. Huang, Reviving the rock-salt phases in Ni-rich layered cathodes by mechano-electrochemistry in all-solid-state batteries, Nano Energy 105 (2023) 108016.
[31] K.R. Tallman, G.P. Wheeler, C.J. Kern, E. Stavitski, X. Tong, K.J. Takeuchi, A.C. Marschilok, D.C. Bock, E.S. Takeuchi, Nickel-rich Nickel Manganese Cobalt (NMC622) Cathode Lithiation Mechanism and Extended Cycling Effects Using Operando X-ray Absorption Spectroscopy, The Journal of Physical Chemistry C 125(1) (2021) 58-73.
[32] K. Kleiner, C.A. Murray, C. Grosu, B. Ying, M. Winter, P. Nagel, S. Schuppler, M. Merz, On the Origin of Reversible and Irreversible Reactions in $LiNi_xCo_{(1-x)/2}Mn_{(1-x)/2}O_2$, Journal of The Electrochemical Society 168(12) (2021) 120533.
[33] R. Lin, S.-M. Bak, Y. Shin, R. Zhang, C. Wang, K. Kisslinger, M. Ge, X. Huang, Z. Shadike, A. Pattammattel, H. Yan, Y. Chu, J. Wu, W. Yang, M.S. Whittingham, H.L. Xin, X.-Q. Yang, Hierarchical nickel valence gradient stabilizes high-nickel content layered cathode materials, Nature Communications 12(1) (2021) 2350.
[34] A. Pattammattel, R. Tappero, M. Ge, Y.S. Chu, X. Huang, Y. Gao, H. Yang, High-sensitivity nanoscale chemical imaging with hard x-ray nano-XANES, Sci Adv 6(37) (2020).
[35] S.-M. Bak, K.-W. Nam, W. Chang, X. Yu, E. Hu, S. Hwang, E.A. Stach, K.-B. Kim, K.Y. Chung, X.-Q. Yang, Correlating structural changes and gas evolution during the thermal decomposition of charged $Li_xNi_{0.8}Co_{0.15}Al_{0.05}O_2$ cathode materials, Chemistry of Materials 25(3) (2013) 337-351.
[36] Y. Shin, S. Maeng, Y. Chung, G.K. Krumdick, S. Min, Core–Multishell-Structured Digital-Gradient Cathode Materials with Enhanced Mechanical and Electrochemical Durability, Small 17(19) (2021) 2100040.
[37] L. Li, H. Yan, W. Xu, D.T. Yu, A. Heroux, W.K. Lee, S.I. Campbell, Y.S. Chu, PyXRF:

Python-Based X-ray Fluorescence Analysis Package, Proc Spie 10389 (2017).
[38] B. Ravel, M. Newville, ATHENA and ARTEMIS: interactive graphical data analysis using IFEFFIT, Physica Scripta 2005(T115) (2005) 1007.
[39] Z. Shadike, H.-S. Lee, C. Tian, K. Sun, L. Song, E. Hu, I. Waluyo, A. Hunt, S. Ghose, Y. Hu, J. Zhou, J. Wang, P. Northrup, S.-M. Bak, X.-Q. Yang, Synthesis and Characterization of a Molecularly Designed High-Performance Organodisulfide as Cathode Material for Lithium Batteries, Advanced Energy Materials 9(21) (2019) 1900705.

Highlights

- Concentration gradient $LiNi_{0.6}Mn_{0.2}Co_{0.2}O_2$ (CG NMC622) cathode material exhibits better cycling stability and thermal stability compared to the conventional NMC622.
- The multi-scale spectroscopy studies revealed that the Mn-rich surface of CGNMC622 promotes an Mn-O-rich surface and helps maintain Ni-redox species during cycling.
- The Mn-O-rich surface suppresses the oxygen release at the charged state, which makes the LIBs much safer.

Graphical Abstract

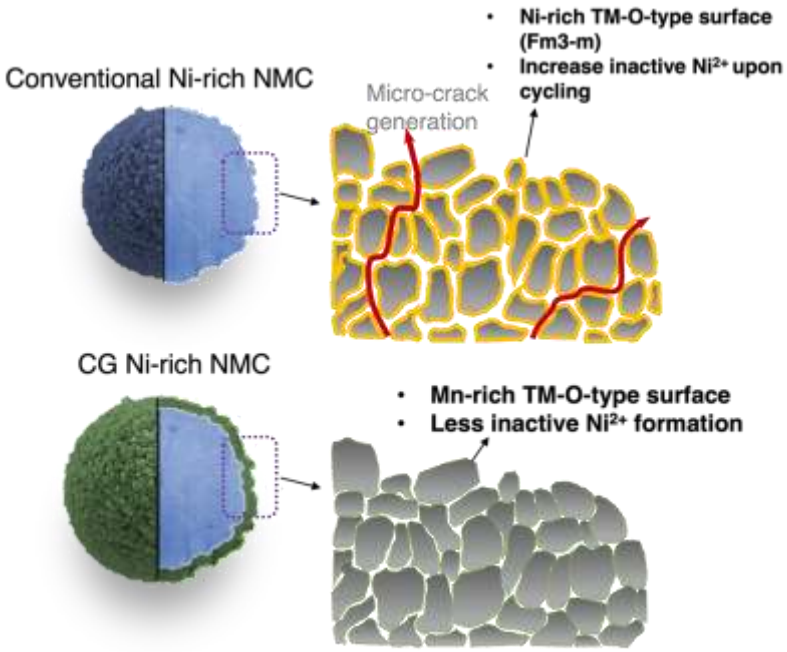

Declaration of interests